# FIRING DEFORMATION IN LARGE SIZE PORCELAIN TILES. EFFECT OF COMPOSITIONAL AND PROCESS VARIABLES

**E. Sánchez[(1)], V. Sanz[(1)], M.C. Bordes[(1)], J. Sales[(2)], K. Kayacı[(3)], M.U. Taşkıran[(3)], Ü.E. Anıl[(3)], Ş. Türk[(3)] , M. Tarhan [(3)]**

**[((1)] Instituto de Tecnología Cerámica (ITC). Universitat Jaume I. Castellón (Spain)**

**[(2)] GEA CERAMICA S.L, Castellón (Spain)**

**[(3)] Kaleseramik Canakkale Kalebodur, Çan (Turkey)**

## 1. INTRODUCTION

The manufacture of porcelain stoneware has undergone a spectacular growth in the last years, as a result of the good technical and functional performance associated to the impervious feature of the sintered product, together with the great technological advance that the ceramic tile manufacturing sector is experiencing [1]. To such an extent, that today, porcelain stoneware is the most demanded product for use in flooring surfaces, but at the same time, it is becoming important to incorporate in other applications such as ventilated facades.

The lack of planarity in porcelain tiles represents a group of defects that remarkably reduce the quality of the finished product. The origin for this problem can be diverse: wrong fit between glaze and body, inadequate firing and pyroplastic deformation [2]. Assuming an adequate firing process, the other two causes are certainly related to both materials and manufacturing process. While the curvature problem associated to the mismatch between body and glaze has extensively reported in the literature for different types of tiles [3], research on pyroplastic deformation phenomenon has mainly focused on whitewares products (tableware, sanitaryware, etc) [4],[5]. Despite the interesting findings reported by all this research, it should be noted that firing of whitewares is commonly carried out at much longer cycles than those used in porcelain tile manufacturing, therefore these findings are not easily extrapolable.

Porcelain tile starting composition is made from a triaxial mixture of clay or kaolin, quartz, and feldspar. The clay fraction helps forming by providing plasticity and dry mechanical strength during processing, and develops mullite and mainly glassy phase when firing. Feldspars develop glassy phase at low temperatures (sodium feldspar being mainly used), assisting the sintering process, and enabling virtually zero (<0.5%) open porosity and a low level of closed porosity (<10%) to be achieved. Quartz promotes thermal and dimensional stability thanks to its high melting point [6].

During firing a porcelain tile body, above 950-1000ºC a viscous liquid phase develops, which is responsible for the vitrifying (densification) process. From this temperature on, the tile material no longer behaves as rigid solid and, if a mechanical stress is applied, a permanent deformation called pyroplastic deformation takes place [7][8]. The degree of deformation depends on the apparent viscosity of the system, which has to do with the amount of liquid phase and its viscosity as well as with the mechanical stress applied. During the firing reactions in typical industrial kilns (single layer rollers kiln) the tile must retain its dimensional characteristics as it advances through the kiln. However, it has become increasingly difficult due to the recent innovations in porcelain tile manufacture, such as thin thicknesses, very large formats and faster firing cycles. Pyroplastic deformation can already be visible at the kiln exit as a small collapse at the tile edges produced during the soaking time at the maximum firing temperature. The body composition and the process parameters should be therefore carefully selected, so as to achieve low porosities at short firing cycles without deformation of the tile.

In a paper on planarity of floor tiles Escardino et al [9] reported that at equal composition and by maintaining the process variables before firing constant, the tendency to pyroplastic deformation is related only to the porosity of the fired tile. These authors also pointed out that the most effective method to reduce the deformation of the tiles is to increase the green density of the tile after pressing. Although the paper set out a complete analysis of the process variables affecting pyroplastic deformation the research was based on a specific redware ceramic composition which characterizes by a much lower firing temperature and different sintering behaviour. In another work Bernandin et al [10] used a mixture design to formulate porcelain tile compositions resistant to pyroplastic deformation. By statistical analysis the authors concluded that, as expected, albite from sodium feldspar is the main phase affecting pyroplastic deformation during firing while iron oxide from clay also causes a strong influence. More recently Bresciani and Spinelli examined the factors that determine the tendency of porcelain bodies to undergo pyroplastic deformation [11]. The study presented several porcelain compositions and an instrumental analysis of pyroplasticity. These authors highlighted the effect of the sodium/potassium ratio in the feldspar raw materials as well as the importance of keeping a minimum quartz content in the fired body which acts as skeleton for the piece microstructure. Moreover, the authors insist on the need to use an appropriate firing cycle with relation to the size/thickness ratio of the manufacturing tile. In a more recent paper, L. dos Santos et al [12] compared the pyroplastic deformation of porcelain tile bodies obtained from wet and dry milling. On one hand the paper emphasized the importance of the combination of micronized quartz and feldspar to optimize sintering rate without compromising the planarity of the tile. On the other hand, the paper also showed the influence of tile microstructure homogeneity on pyroplastic deformation.

Despite the existence of many studies on porcelain tiles reporting the relationship between the content and nature of the glassy phase and the sintering rate [7],[8],[13] a clear relation between starting composition features and pyroplastic deformation has not been addressed yet. In addition, the effect of some fluxing materials typically added to porcelain tile composition to enhance sintering rate such as alkaline-earth containing raw materials (calcium carbonate, magnesite, dolomite, etc.) have scarcely been considered. The addition of this type of materials produces an expected decreasing of sintering temperature together with in more or less extent a shortening of the firing range as a consequence of the decreasing in the viscosity of the glassy phase associated with the incorporation of the alkaline-earth oxide in the melting. For this same reason, an effect of alkaline-earth fluxing material on the pyroplastic deformation should be expected.

From the above it can be inferred that, due to the lack of research activity on the pyroplastic deformation in porcelain tiles as well as the growing interest on firing deformation problems in this type of products, there is a need to raise a study to shed light on this subject. On one hand, this research will address the effect of the main process variables in porcelain tile manufacture, i.e body particle size and unfired bulk density of the pressed tile on the tendency to deformate by pyroplasticity. The interaction of both variables needs to be considered. On the other hand, the paper will also analyze the effect of different alkaline-earth raw materials used in the industrial practice on this same tendency. The final objective of the research is to contribute to establish a more robust process conditions for manufacturing large format porcelain tiles without firing deformations.

## 2. MATERIALS AND METHODS

Typical raw materials used in the industry to manufacture porcelain tiles were used: Ukrainian clay, Turkish sodium feldspar and feldsphatic sand. Together with these main raw materials other alkaline-earth fluxing additives were used: Calcite (C), Dolomite (D), Magnesite (M) and Talc (T). Table 1 collects the chemical and mineralogical composition of all these materials determined by X-ray fluorescence (XRF) and X-ray diffraction (XRD), respectively. The DTA-TGA tests were also carried out for fluxing materials. The tests were performed in a Mettler TGA/STDA 815e thermobalance at a heating rate of 10 K/min.

| Elements | Clay | Feldspar | Feldspathic sand | Dolomite | Calcite | Magnesite | Talc |
|---|---|---|---|---|---|---|---|
| $SiO_2$ | 66.00 | 69.00 | 89.60 | 0.20 | 0.29 | 8.21 | 46.00 |
| $Al_2O_3$ | 22.10 | 18.90 | 6.40 | 0.38 | 0.15 | 1.71 | 10.50 |
| $Fe_2O_3$ | 0.93 | 0.16 | 0.13 | 0.03 | 0.05 | 0.45 | 1.90 |
| CaO | 0.30 | 0.82 | 0.10 | 33.64 | 55.6 | 1.67 | 1.10 |
| MgO | 0.54 | 0.16 | 0.07 | 18.61 | 0.10 | 41.20 | 31.00 |
| $Na_2O$ | 0.40 | 9.70 | 0.25 | 0.20 | - | 0.15 | 0.10 |
| $K_2O$ | 2.16 | 0.38 | 2.46 | 0.06 | - | 0.10 | 0.10 |
| $TiO_2$ | 1.45 | 0.32 | 0.10 | 0.09 | - | 0.19 | 0.20 |
| $P_2O_5$ | 0.05 | 0.20 | - | - | - | .. | - |
| $SO_3$ | 0.02 | - | - | - | - | | - |
| L.O.I. | 6.04 | 0.34 | 0.86 | 46.39 | 43.40 | 45.50 | 9.60 |
| Mineralogical phases | K | A | Q | D | C | M | T |
| | Q | I | K | - | - | Q | D |
| | I | Q | O | - | - | Mo | Ch |
| | Others | Others | Others | - | - | - | - |

***Table 1.*** *Chemical and mineralogical composition of all the raw materials used. Chemical composition is given in wt%.*

*A → Albite*
*C → Calcite*
*Ch → Chlorite*
*D → Dolomite*
*I → Illite + Mica Muscovite*
*K → Kaolinite*
*M → Magnesite*
*Mo → Montmorillonite*
*O → Orthoclase*
*Q → Quartz*
*T →Talc*

From these raw materials, a standard composition made up of clay (40 wt%), sodium feldspar (35 wt%) and feldesphatic sand (25 wt%) was formulated. From this composition some series of compositions incorporating different proportions of the alkaline-earth additives were prepared. A wide variation of the proportion of each fluxing additive was assessed in an attempt to provoke significant changes in the sintering behaviour of the standard composition. Table 2 shows the addition range to the standard composition for each fluxing material. The reference used for the different compositions is also denoted in the table. The procedure followed to prepare the ceramic powder from all the compositions has been explained elsewhere [9],[14],[15]. A fixed grinding oversize was established for all the compositions in order to keep constant the particle size distribution of powders. This residue was 6 wt% over 40 μm sieve.

| Fluxing additive | Composition reference | Compositional range (weight %) | Fluxing oxides* (mol).$10^3$ |
|---|---|---|---|
| Calcite | C | 2.10 – 7.00 | 20.9 - 69.6 |
| Dolomite | D | 1.05 – 5.00 | 11.1 – 53.1 |
| Magnesite | M | 0.35 – 1.05 | 3.7 – 11.0 |
| Talc | T | 0.94 – 3.50 | 7.4 – 27.6 |

* MgO + CaO

***Table 2.*** *Addition range to the standard composition for each fluxing material. References of the compositional series are also indicated.*

With a view to assessing the effect of particle size of porcelain tile body composition, the standard (STD) mixture was ground in a laboratory, planetary mill at three different residues over 40 μm sieve: 1, 3 and 6 wt%.

To determine pressing and firing behaviour, cylindrical test pieces about 5 mm thick and 50 mm in diameter were formed. In addition, test pieces measuring 80x20x6 mm, were prepared to determine the pyroplasticity index. Regardless the geometry of the pieces, the bodies were formed at a moisture content of 6% (on a dry basis) by uniaxial pressing at a pressure of 400 kg/cm$^2$. In some cases, this pressing pressure was varied (increased or decreased) when compositions with different particle size or fluxing additive had to be formed at constant bulk density. After they had been pressed, the test pieces were sintered in an electric laboratory kiln with a heating ramp of 70 °C/min between 25 °C and 500 °C, and 25 °C/min from 500 °C to the respective peak firing temperature. The residence time at peak firing temperature was 6 minutes. The peak firing temperatures encompassed the range 1170–1240 °C, depending on each composition.

The technological properties of the fired test pieces were evaluated by performing the following tests: linear shrinkage, bulk density and water absorption. Bulk density was measured using the mercury displacement method; firing shrinkage was assessed as the difference between dry and fired diameters, defining these parameters on a dry basis. Water absorption was performed by the impregnation method under vacuum. In this method, the water uptake is calculated by measuring the gain in test piece weight, after being subjected to a vacuum pressure of 91 kPa for 30 minutes, then being submerged in water and then remaining in the water at atmospheric pressure for 15 minutes.

In order to determine the tendency to deform by pyroplasticity, prism-shaped test specimens were fired at different maximum temperatures in an electric laboratory kiln. To perform the firing, the test specimens only rested on their two ends, thus allowing them to deform in the course of firing [9]. Their tendency to deform by pyroplasticity was evaluated by calculating the pyroplasticity index (PI) from the following expression:

$$IP = \frac{4 \cdot e^2 \cdot s}{3 \cdot L^4}$$

where: e = body thickness, s = sag (body firing deformation) and L = body length.

The sintering behaviour of the compositions was characterized by using a MISURA hot stage microscope. The hot stage microscope allows a sample to be visualised when it is put through a heating cycle. The computer concurrently records the sample silhouette during the melting test. The recorded images enable the evolution of sample shrinkage with temperature to be determined with an image analyser. To perform the test, the powder was pressed to form a 3-mm-high cylindrical button with a 3-mm diameter. This was set on an alumina base in the hot stage microscope sample holder, and subjected to a heating cycle at a rate of 25 ºC/min. The characteristic temperatures determined from the recorded images are shown in Table 3 [6],[16].

| Temperature | Viscosity (dPa.s) | Temperature | Viscosity (dPa.s) |
|---|---|---|---|
| Initial temperature (TI) | $10^{\infty}$ | Softening point (TSP) | $10^{6}$ |
| First shrinkage (TFS) | $10^{12}$ | Half ball (THB) | $10^{4.5}$ |
| Maximum shrinkage (TMS) | $10^{10}$ | Flow point (TFP) | $10^{3}$ |

***Table 3.*** *Characteristic temperatures and the corresponding estimated viscosities from the recorded images at the hot stage microscope.*

## 3. RESULTS AND DISCUSSION

### 3.1. THERMAL BEHAVIOUR OF ADDED FLUXING MATERIALS

Table 4 shows the DTA-TGA tests results for the four fluxing materials used in this research. For carbonates samples (calcite, dolomite and magnesite) the thermal behaviour corresponds to that of almost pure substances, exhibiting exclusively the endothermic peaks associated to the carbonate decomposition, one peak for C and M samples and two peaks for D. Besides, when compared the three carbonates, it is noticeable the much lower decomposition temperature of magnesite (see Table 4) which can make the gas removal during a fast firing cycle easier. Unlike the carbonates, talc sample displays a more complex thermal behaviour as a consequence of the existence of other minerals in the sample together with talc crystalline structure. Thus, apart from the water removal from talc crystalline network breakdown observed at 964 ºC, there are other two decompositions corresponding to chlorite mineral and dolomite.

| Fluxing material | Temperature (ºC) | Thermal event |
|---|---|---|
| Calcite | 889 | $CaCO_3$ Decomposition |
| Dolomite | 825-920 | $MgCO_3$-$CaCO_3$ Decomposition |
| Magnesite | 652 | $MgCO_3$ Decomposition |
| Talc | 633 | (1) Chlorite dehydration |
| | 800-850 | (2) Dolomite decomposition |
| | 964 | (3) Talc dehydration |

***Table 4**. Characteristic temperatures and thermal events for the fluxing materials studied.*

## 3.2. INFLUENCE OF MAIN PROCESS VARIABLES (COMPOSITION PARTICLE SIZE AND UNFIRED BODY BULK DENSITY) ON FIRING BEHAVIOUR AND PYROPLASTIC DEFORMATION

Figure 1 plots the firing diagram (fired bulk density and water absorption versus firing temperature) for the STD composition milled at the three oversizes of 1, 3 and 6 wt% (hereafter named 1-STD, 3-STD and 6-STD). To eliminate the effect of the particle size distribution on particle packing when pressing this diagram was obtained for pressed bodies formed at constant unfired bulk density of 1.94 g/cm$^3$. Thus, for 1-STD higher pressure than 400 kg/cm$^2$ was necessary while the contrary was true for 6-STD composition. As expected, a finer particle size gives rise to a decrease of the maximum densification temperature (an increase of sintering rate) as well as the temperature at which the water absorption reaches zero value. Additionally, decreasing particle size also leads to higher densification values. As previously reported, when the particle size decreases a tile microstructure made up of finer pores and higher reactivity (increasing number of contacts between solid particles) develops enhancing densification process [17].

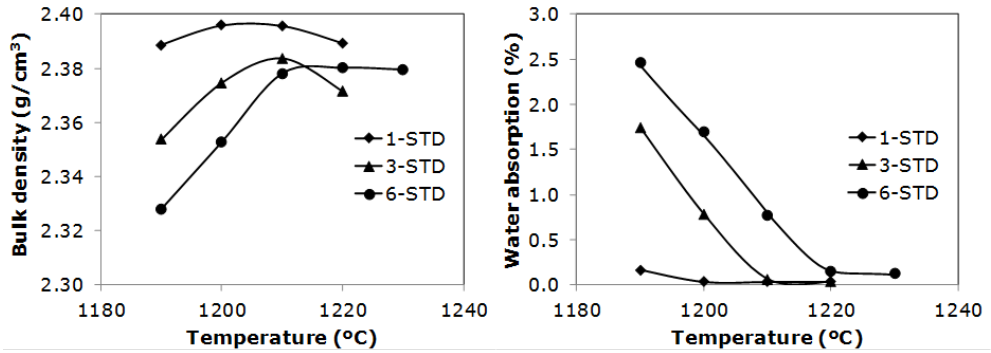


***Figure 1.** Variation of fired bulk density (a) and water absorption (b) versus firing temperature for 1-STD, 3-STD and 6-STD compositions (bulk density of 1.94 g/cm$^3$).*

Figure 2 shows micrographs of fired bodies obtained from 1-STD, 3-STD and 6-STD samples. As observed, the micrographs corroborate the variation of microstructure with grinding time set out above. However, increasing grinding time also produces narrower particle size distributions which impair particle packing [18] as deduced from the bulk density values in Table 5 corresponding to bodies pressed from these three compositions at the same pressing conditions (6 wt% humidity content and 400 kg/cm$^2$ pressing pressure).

| Composition | Unfired bulk density (g/cm$^3$) |
|---|---|
| 1-STD | 1.90 |
| 3-STD | 1.94 |
| 6-STD | 1.97 |

***Table 5.*** *Unfired bulk density for 1- STD, 3-STD and 6-STD composition pressed at the same pressing conditions.*

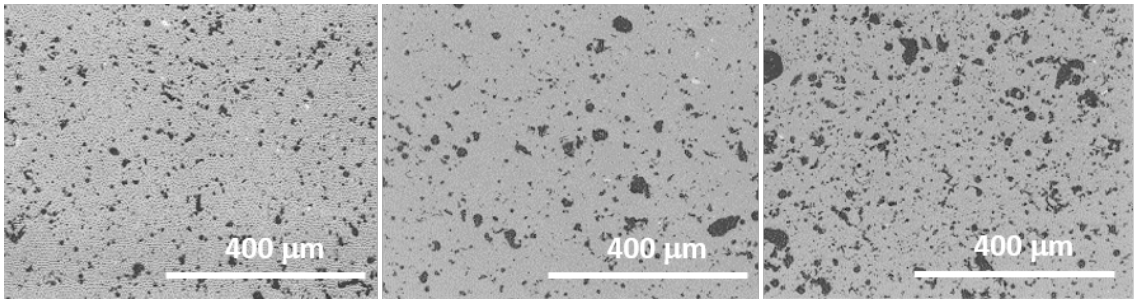


***Figure 2.*** *Microstructure of fired body specimens sintered at the maximum densification temperature obtained from 1-STD, 3-STD and 6-STD compositions (from left to right).*

The analysis of the pyroplastic deformation has been done by plotting pyroplastic index against water absorption as suggested by Escardino et al [9]. Figure 3 shows this representation for 1-STD, 3-STD and 6-STD compositions. Due to the interaction of composition particle size on unfired bulk density two types of representation have been drawn: the variation of pyroplastic index with water absorption for bodies pressed at the constant pressing conditions set out in Table 5 (Figure 3a) and the same plot but for bodies pressed at the constant unfired bulk density of 1.94 kg/cm$^3$ (Figure 3b). As it can be observed, all the curves show the expected hyperbolic-like variation (increase) of pyroplastic index as the water absorption decreases. As postulated by these authors with a red-firing floor tile composition, as the temperature rises to obtain low water absorption the densification rate (variation of water absorption with time) by liquid-phase sintering gradually decays while deformation rate (variation of pyroplastic index with time) rapidly grows leading to a strong increment of pyroplastic deformation. On the other hand, as a consequence of the tile microstructure obtained from the three compositions (see Figure 2), a reduction of pyroplastic deformation (PI) as well as of the slopes of the curve at constant water absorption with increasing grinding time should be expected as reported in the previous research with redware floor tile composition [9]. However, despite the significant differences provoked in the particle size distribution of the compositions, PI values for the coarsest particle size composition are much lower than those of the finest particle

size composition. In fact, PI values increase according to the following sequence 1-STD > 3-STD > 6-STD. This is because, as mentioned above, milling time affects to both reactivity of the powder and bulk density of the pressed tiles. Finer particle size decreases firing temperature while the same is true when the pressed tile bulk density rises. Consequently, increasing milling time produces two simultaneous and opposing effects on vitrification temperature and pyroplastic index which explains the unexpected sequence of the curves of pyroplastic trend variation with water absorption shown in Figure 3a. As mentioned, this finding contrasts with that observed for redware floor tile composition in which the particle size effect prevailed over the bulk density effect, that is, a contrary sequence as that set out above was reported [9].

These findings can be confirmed when analysing Figure 3b where the plot of pyroplastic index versus water absorption was determined for constant bulk density bodies. As it can be observed, when the bulk density in the pressed tiles keeps constant the effect of particle size distribution on pyroplastic index becomes evident. Thus, as it could be expected, decreasing particle size gives rise to a dramatic reduction of the pyroplastic deformation trend, the effect is much more pronounced as the water absorption approaches 0. Thus, the variation of IP values for a given water absorption follows the expected sequence: 6-STD > 3-STD > 1-STD. From these findings, it can be easily deduced that the join effect of coarse particle size and low bulk density can be detrimental for the appearance of pyroplastic deformation problems. Thus, these results emphasize the importance of particle size and bulk density regarding pyroplastic deformation as well as the need to control these parameters during the manufacturing process. On the other hand, in the industrial practice, milling time, and consequently, particle size distribution usually is kept constant for the implications that this parameter has on many other process parameters. For this reason, it is much more advisable and easier to act on the pressing bulk density to adjust the firing behaviour of the tile in terms of densification and deformation rate.

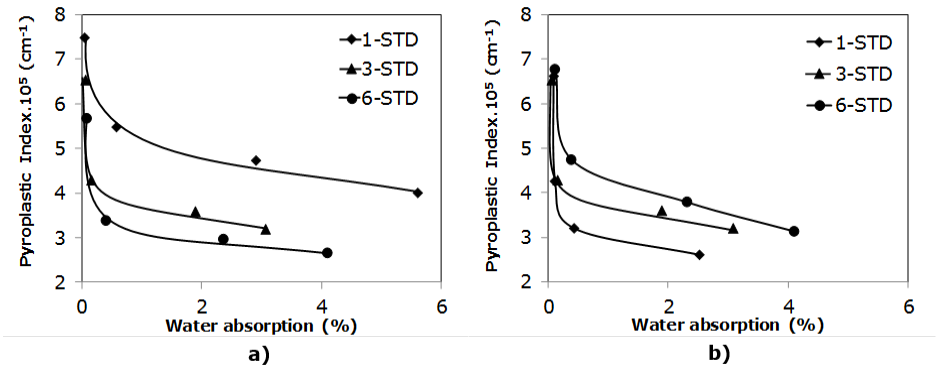


***Figure 3.*** *Variation of PI versus water absorption for 1-STD, 3-STD and 6-STD compositions formed at a) the same pressing pressure of 400 kg/cm$^2$ and b) the same unfired bulk density (1.94 g/cm$^3$).*

### 3.3. INFLUENCE OF THE NATURE AND AMOUNT OF FLUXING ADDITIVES ON FIRING BEHAVIOUR AND PYROPLASTIC DEFORMATION

Four typical fluxing additives were assessed. Each fluxing material has been tested at three different addition percentage trying to cover the amount used in the industrial practice, and, more interestingly, allowing the composition to reach and overcome the maximum densification state at a reasonable firing temperature. In all the cases, the reference used to denote each composition was as follows: additive initial-weight percentage. Thus, for example, a composition with an addition of 0.7 wt% of Magnesite is denoted by M-0.7. Moreover, the unfired bulk density was kept constant for all the pressed specimens (1.97 g/cm$^3$) by modifying the pressing pressure when necessary. Therefore, in the following discussions the effect of this parameter will be disregarded.

The firing diagrams for each series of compositions are shown in Figure 4 and Figure 5. In these figures, the curve corresponding to the standard composition with the same unfired bulk density of 1.97 g/cm$^3$ (6-STD) is included for the sake of comparison. On observing these graphs the role of the fluxing material (alkaline-earth oxides) of the four compounds is evident, i.e in all the cases the addition of the fluxing material shifts, in more or less extent, the firing curves (fired bulk density and water absorption) to the left (lower firing temperatures). On the other hand, maximum firing density is practically not affected for M and T compositions while for D and C series, specifically for the highest amount of fluxing material addition, maximum firing density and, above all, bulk density curve profiles are strongly altered. It is particularly noticeable the narrowing effect on the densification curves produced by the increasing addition of Dolomite. A reason for this effect is not clear, but probably the porosity increase at relatively high temperature during firing from the decomposition of dolomite (as observed in the DTA results in Table 4) can contribute, in some extent, to this behaviour. Another possible explanation for this shortening of the firing range could be related to a sort of alkaline-earth mixing effect from calcium-magnesium mixture similar to that widely explained in glass literature for alkaline oxide mixtures [19]. This effect has been recently reported for Ca-Mg silicate glasses, confirming the non-linear evolution of compositional dependence for viscosity in these glasses [20]. Nevertheless, this hypothesis should be confirmed with further research by using standard porcelain tile compositions. In the case of calcite addition, there is a strong impact on densification curve for the highest (7 wt%) addition. For this C-7 composition maximum firing density is not reached as a consequence of a significant delay in the densification process. As reported elsewhere, increasing addition of calcium supplying raw materials to an alumino-silicate ceramic mixture gives rise to the formation of calcium-based crystalline phases such as anorthite and wollastonite which are responsible for this densification retardation [21],[22].

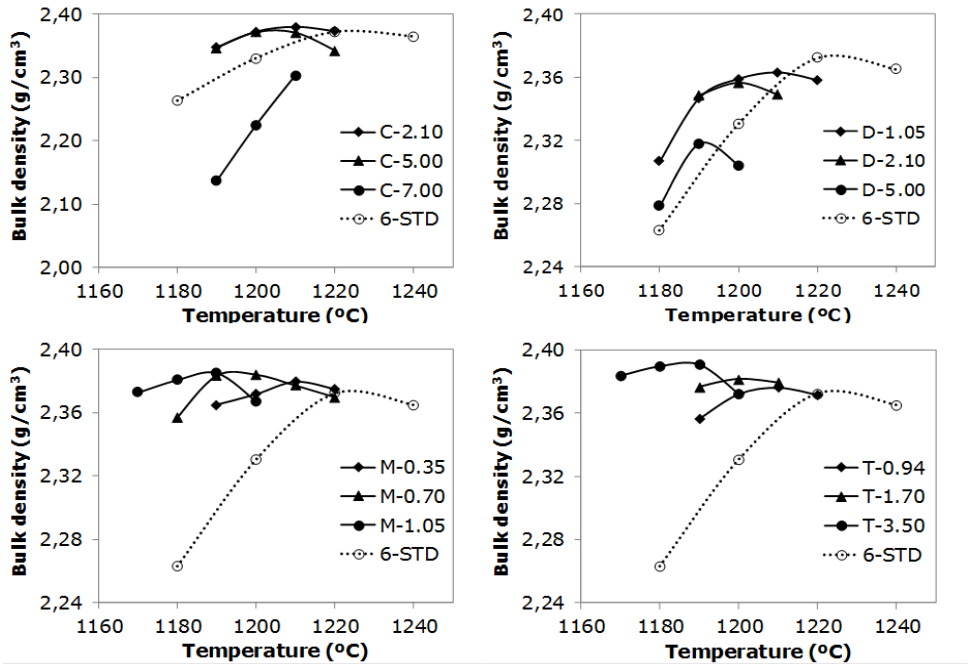


***Figure 4.*** *Variation of fired bulk density versus firing temperature for the four series of compositions: C, D, M and T.*

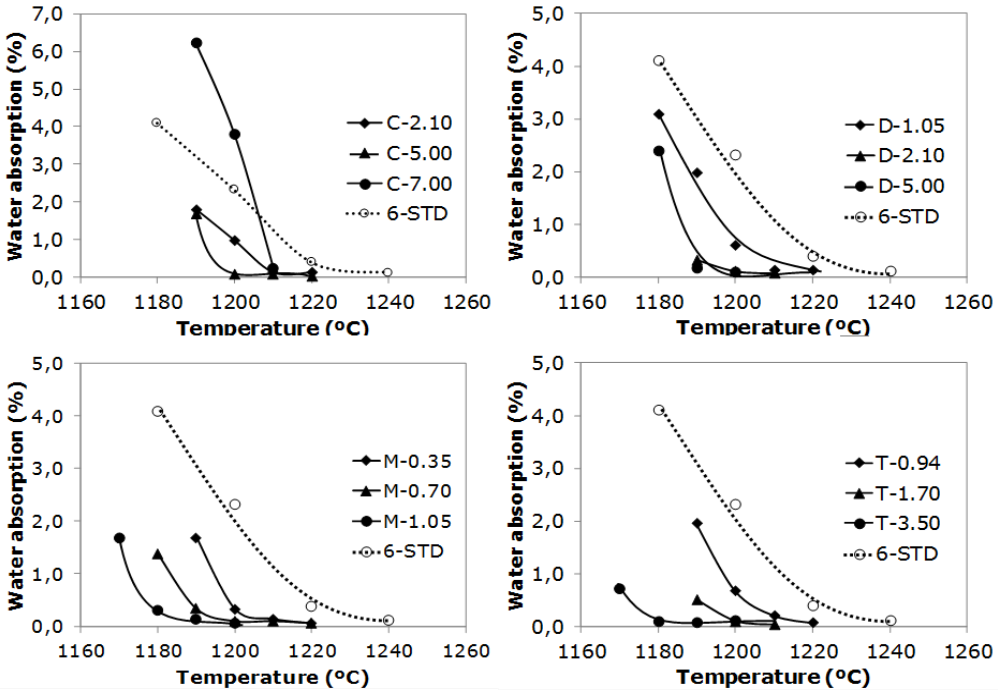


***Figure 5.*** *Variation of water absorption versus firing temperature for the four series of compositions: C, D, M and T.*

With regard to the efficiency of the different fluxing materials, a simple observation of the four diagrams allows us to conclude that magnesite leads to the same effect with much lower amount of additive. In Table 6 it can be observed the efficiency of a normalised amount of additive (2 wt% for all the compositions except 1 wt% for magnesite) in terms of decrease of maximum density temperature. For a more rigorous comparison a third column in the table details the molar amount of fluxing oxide supplied by each of these additives. As observed, all the compounds supply similar molar amounts of fluxing oxides except talc, as a consequence of its much more different chemical nature [23]. From all these data, the additives can be easily ordered according to the decreasing fluxing efficiency as follows: magnesite>talc>dolomite>calcite. In the table the molar amount of volatile inorganic substances is also included.

| Fluxing additive | ΔT (ºC) | Fluxing oxides (mol) . $10^3$ | Volatile substances (mol). $10^3$ |
|---|---|---|---|
| Calcite (2%) | 2 | 19.9 | 19.7 |
| Dolomite (2%) | 10 | 21.2 | 21.1 |
| Magnesite (1%) | 23 | 10.5 | 10.2 |
| Talc (2%) | 16 | 15.8 | 5.1 |

***Table 6.*** *Efficiency of the four fluxing materials tested in terms of decrease of maximum firing density temperature (ΔT). For comparison purpose, the molar amount of fluxing oxides (MgO+CaO) supplied by each of these substances is included in the table.*

In order to try to understand the reasons for this different firing efficiency of the fluxing materials the sintering behaviour of one composition of each composition series was determined. The selected sample corresponded to the intermedium addition of each fluxing agent, i.e: C-5, D-1.7, M-0.7 and T-1.7. The test was carried out in the hot stage microscope as set out above. The shrinkage versus temperature curves of each composition is shown in Figure 6a. For comparison purpose, the curve corresponding to 6-STD composition (6 wt% oversize) is also included. As it can be observed all the compositions show similar sintering profiles where the body shrinkage (sintering) starts to be significant over 1050 ºC. Then, the sintering proceeds very rapidly in all the cases until a maximum shrinkage temperature around 1240ºC ºC. This behaviour corresponds with the liquid-phase sintering mechanism occurring during firing of typical porcelain tile bodies as reported elsewhere [1],[7],[8],[24]. When comparing the four curves it can be observed that for calcite composition all the significant changes in the sintering process take place earlier: shrinkage start, maximum shrinkage and contraction start (deformation). For the other three compositions, the curves more or less coincide. Finally, the 6-STD composition is shifted to the right (higher temperatures) as expected due to the inexistence of any fluxing additive. Assuming that a standard porcelain tile composition can contain till 50-60 wt% of amorphous phase in the fired state [8],[12], the influence of the amount and nature of this liquid phase becomes evident. For this reason, from the hot stage

microscope findings, viscosity versus temperature curves were calculated according to the specific viscosity points shown in Table 3 and literature data [6],[16]. It should be noted that this is a rough estimate of the viscosity of the assumed liquid phases developing in the composition during the firing treatment. Figure 7b displays these estimated curves. As it can be observed, all the curves exhibit a similar profile where a dramatic reduction of viscosity with temperature occurs for temperatures higher than 1250 ºC. In all the cases, the fluxing addition leads to the reduction of viscosity (the curves shift to the left) in comparison with the STD composition. The decrease in viscosity, i.e, the displacement to lower temperatures for the curves follows a relationship with the amount of fluxing material added to the composition: C-5> D-2.1> T1.7> M-0.7, indicating that, regardless the nature of the fluxing material, the amount of fluxing agent added to the composition defines the viscosity of the melting phase developed during firing. This finding is consistent with viscosity estimates for homogeneous glasses which exhibit a significant reduction of viscosity as small amounts of alkaline or alkaline-earth oxides replace silica in the glass network [19].

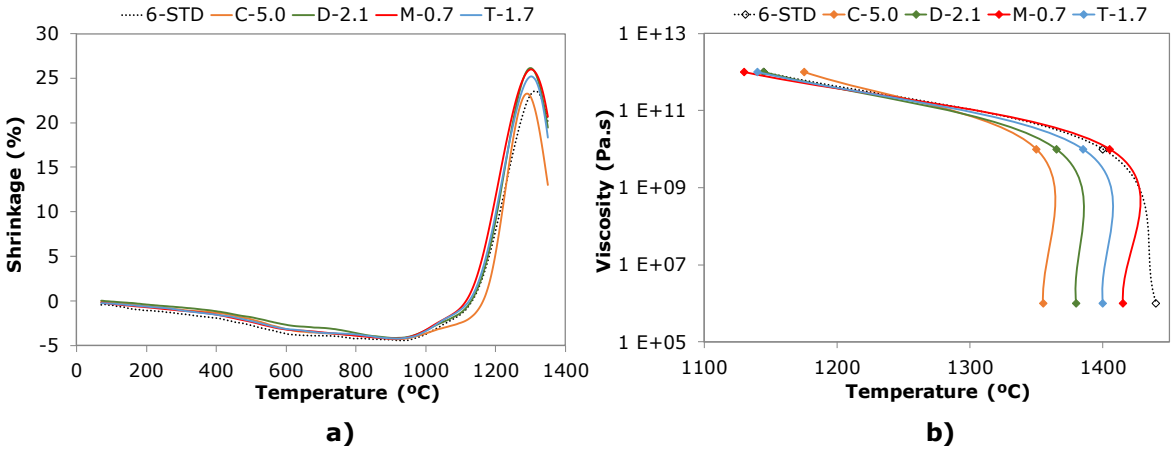


***Figure 6.*** *Hot stage microscope: a) Densification curve and b) Curve of estimated viscosities with temperature according to Table 3.*

From the findings above it can be deduced that there is not a clear correspondence between liquid-phase viscosity and firing efficiency of the fluxing material. Nevertheless, when comparing Figures 4, 5 and 6 some interesting conclusions can be inferred. Firstly, magnesium fluxing materials (magnesite and talc) are much more efficient in terms of firing temperature reduction than calcium supplying additives (dolomite and calcite). Secondly, the low viscosity provided by the calcite composition seems to be compensated by the crystallization of the calcium oxide-alumina-silica phases as reported elsewhere. This fact is corroborated by the curve profile of the C-7 composition in which the formation of crystalline phases which retard sintering process is quite evident.

Figure 7 shows the diagram of pyroplasticiy index versus water absorption for all the specimens prepared from the four compositions together with the 6-STD composition. As it can be seen, all the composition display the variation profile already shown in the previous section, i.e a hyperbolic-like increase of pyroplasticity as the water absorption approaches zero. At low, typically porcelain

tile water absorptions (below 0.5%) all the compositions present higher pyroplasticity values than those of the 6-STD composition.

For the C-5 composition the effect is minimum at higher water absorptions which is consistent with the lower fluxing efficiency of this additive. On the contrary, the increase in the pyroplasticity index is much higher for the dolomite composition than for the other three. This finding agrees with the results set out in the firing diagrams where the detrimental effect of dolomite addition on the firing range of the composition was observed. This relationship between the firing range shortening effect and pyroplastic deformation has been also reported in previous research with more fluxing tile compositions [9].

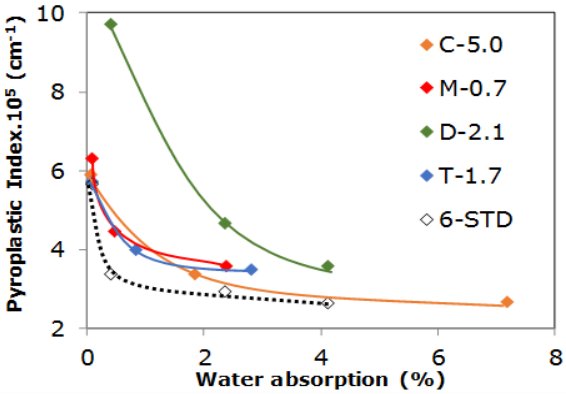


***Figure 7.*** *Variation of pyroplastic index versus water absorption for bodies obtained from C-5.0, D-2.1, M-0.7, T-1.7 and 6-STD compositions.*

If firing efficiency as shown by reduction of vitrification temperature (Figure 4 and 5 and Table 6) and firing deformation as represented by pyroplastic index variation with water absorption (Figure 7) are taken into account, it can be concluded that magnesite provides the highest efficiency together with a moderate pyroplastic deformation increase when added to a standard porcelain tile composition. Talc can be also a good alternative to magnesite [23]. Nevertheless, calcite effect requires high amount of addition which can give rise to undesirable phases crystallization. Finally, dolomite produces a clear narrowing of the firing range as well as a strong increment of pyroplastic index which make this raw material less attractive to be used in industrial practice.

## 4. CONCLUSIONS

The following conclusions can be inferred from this work:

Bulk density exerts a significant effect on pyroplastic deformation. This is because, when bulk density rises, the number of contacts between particles also grows, while pore volume and size of the pressed tile are reduced. All these facts lead to a diminution of the firing temperature to reach a specific water absorption value.

If the bulk density of the pressed bodies is not kept constant increasing grinding time (lowering composition particle size) does not lead to a reduction of pyroplastic deformation despite the decrease of vitrification temperatures which occurs. This is because milling time enhances powder reactivity but the bulk density of the pressed tile worsens. If the bulk density keeps constant, reduction of composition particle size gives rise to the expected effect on pyroplastic deformation. Thus, the join effect of particle size and bulk density is of paramount importance to avoid pyroplastic deformation problems. This research emphasizes the need to control these parameters during the manufacturing process.

Four typical fluxing additives were assessed in terms of firing behaviour and pyroplastic deformation. The additives were calcite, dolomite, magnesite and talc. Each fluxing material has been tested at different addition percentage trying to cover the amount used in the industrial practice. It was observed that magnesite provides the highest firing efficiency (decreasing of maximum densification temperature) with a moderate pyroplastic deformation increase. Talc can be also a good alternative to magnesite. However, calcite effect is only observable for high additions and its use can give rise to undesirable crystalline phases development. Dolomite was proved not to be a good candidate as fluxing additive because this material produces a significant narrowing of the firing range as well as a strong increment of pyroplastic index. Some reasons for this unusual dolomite performance are given in the paper.

## 5. REFERENCES

[1] E. Sánchez, J. García-Ten, V. Sanz, et al., Ceram. Int. 36(2010) 831-845.

[2] J.L. Amorós, V. Beltrán, A. Blasco, et al., Defectos de fabricación de pavimentos y revestimientos cerámicos. Castellón: Instituto de Tecnología Cerámica, D.L. 1991.

[3] J.L. Amorós, F. Negre, A. Belda, et al., Tec. Ceram. 178(1989) 582-592.

[4] W.M. Carty, Whitewares Mater.: Ceram. Eng. Sci. Proc. 24(2003) 108-132.

[5] D.Y. Tunçel, E. Özel, Ceram. Int. 38(2012) 1399-1407.

[6] A. Barba, V. Beltrán, C. Felíu, et al., Materias primas para la fabricación de soportes de baldosas cerámicas. 2ª ed. Castellón: Instituto de Tecnología Cerámica, 2002.

[7] C. Zanelli, M. Raimondo, G. Guarini, et al., J. Non Cryst. Solids 357(2011) 3251-3260.

[8] E. Sánchez, M.J. Orts, J. García-Ten, et al., Am. Ceram. Soc. Bull. 80(2001) 43-49.

[9] A. Escardino, J.L. Amorós, F. Negre, et al., Interbrick 5(1989) 26-31.

[10] A.M. Bernardin, D. de Medeiros, H.G. Riella, Mat. Sci. Eng. A 427(2006) 316-319.

[11] A. Bresciani, B. Spinelli, CFI Ceram. Forum Int. 89(2012) E41-E45.

[12] L.R. Dos Santos Conserva, F.G. Melchiades, S. Nastri, et al., J. Eur. Ceram. Soc. 37 (2017) 333–342.

[13] D. Magagnin, C.M.F. Dos Santos, A. Wanderlind, et al., Mat. Sci. Eng. A, 618 (2014) 533-539.

[14] J.L. Amorós, E. Sánchez, J. García-Ten, et al., Manual para el control de calidad de materias primas arcillosas. Castellón: Instituto de Tecnología Cerámica-AICE, 1998.

[15] V. Bagán, J.E. Enrique, G. Mallol, et al., Tile & Brick Int. 6(1990) 35-42.

[16] H.R. Lillie, J. Am. Ceram. Soc. 37(1954) 111-117.

[17] J.L. Amorós, M.J. Orts, J. García-Ten, et al., J. Eur. Ceram. Soc. 27(2007) 2295-2301.

[18] E. Sánchez, J. García-Ten, A. Barba, et al., Ceram. Acta, 12(2000) 18-30.

[19] J.M. Fernández Navarro, El vidrio. 3ª de. Madrid: Consejo Superior de Investigaciones Científicas. Sociedad Española de Cerámica y Vidrio, 2003.

[20] Z. Shan, C. Li, H. Tao, J. Am. Ceram. Soc. 100(2016) 4570-4580.

[21] E. Sánchez, J. García, V. Sanz, et al., Tile & Brick Int. 6(1990) 15-21.

[22] J.L. Amorós, A. Escardino, E. Sánchez, et al., Ceram. Inf. 324(1993) 56-67.

[23] V. Biasini, M. Dondi, G. Guarini, et al., Silic. Ind. 68(2003) 67-73.

[24] A. De Noni, D. Hotza, V. Cantavella, et al., Mater. Sci. Eng. A 527(2010), 1730-1735.